Monthly Notices
of the
ROYAL ASTRONOMICAL SOCIETY

MNRAS **490,** 4877–4888 (2019)
Advance Access publication 2019 October 12

doi:10.1093/mnras/stz2873

Dark matter halo shapes in the Auriga simulations

Jesus Prada,[1] Jaime E. Forero-Romero ,[1]★ Robert J. J. Grand ,[2] Rüdiger Pakmor [2] and Volker Springel[2]

[1]*Departamento de Física, Universidad de los Andes, Cra. 1 No. 18A-10, Edificio Ip, Bogotá, Colombia*
[2]*Max-Planck-Institut für Astrophysik, Karl-Schwarzschild-Str. 1, D-85741 Garching, Germany*

Accepted 2019 October 8. Received 2019 October 8; in original form 2019 August 29

ABSTRACT

We present shape measurements of Milky Way–sized dark matter haloes at redshift $z = 0$ in a suite of 30 zoom simulations from the Auriga project. We compare the results in full magnetohydrodynamics against dark matter–only simulations and find a strong influence of baryons in making dark matter haloes rounder at all radii compared to their dark matter–only counterparts. At distances $\lesssim$30 kpc, rounder dark matter distributions correlate with extended massive stellar discs and low-core gas densities. We measure the alignment between the halo and the disc shapes at different radii and find a high degree of alignment at all radii for most of the galaxies. In some cases, the alignment significantly changes as a function of radius implying that the halo shape twists; this effect correlates with recently formed bulges and is almost absent in the dark matter–only simulations. In a comparison against observational constraints, we find that 20 per cent of haloes in our sample are consistent with observational results derived from the Pal 5 stream that favours an almost spherical shape. Including baryons is a required element to achieve this level of agreement. In contrast, none of the simulations (neither dark matter only nor with baryons) match the constraints derived from the Sagittarius stream that favour an oblate dark matter halo.

Key words: galaxies: evolution – galaxies: formation – galaxies: haloes – dark matter.

1 INTRODUCTION

Our physical picture of the Universe as a whole has been shaped by accurate observations and modelling of our own Galaxy. For instance, the study of the Milky Way's (MW) morphology and its separation into different kinematic components, such as disc and bulge, has been used to support the existence of a dark matter (DM) component surrounding the Galaxy (Olling & Merrifield 2000; Sofue, Honma & Omodaka 2009; Catena & Ullio 2010; Bovy & Rix 2013; Iocco, Pato & Bertone 2015). Explaining the matter budget and kinematic state of the MW also puts constraints on the wider cosmological context, besides testing specific models of galactic evolution.

A detailed study of the full three-dimensional (3D) MW gravitational potential could constrain the properties of the DM halo surrounding our Galaxy and even help to pin down the nature of the DM particle. For instance, the study of fossil records of stellar streams resulting from infalling globular clusters or satellite galaxies that got tidally disrupted by the gravitational potential of the MW could be translated into tight constraints both on the shape of the DM halo in the outer regions of our Galaxy (Johnston 1998; Helmi & White 1999; Tremaine 1999) and the properties of DM substructures, which also depend on the microphysics of a given DM particle candidate.

In any case, the observational constraints on the gravitational potential shape must be confronted against the expectations from different galaxy formation models in the full cosmological context. For instance, in the current paradigm of a cold dark matter (CDM)-dominated universe, galaxies are expected to be hosted by triaxial DM haloes. To what extent are these CDM expectations born out in observations of our Galaxy?

This question has been challenging to address for many years, because it has been difficult to produce realistic galactic discs in simulations within the CDM context (Navarro & Steinmetz 1997). It is now understood that a prerequisite for successful disc formation is an adequate accounting of strong baryonic feedback effects, such as stellar feedback and black hole feedback, because they play an important role in forming late-time galaxies resembling the MW. Along the way, different numerical experiments have also shown that the baryonic effects also impact the DM halo shape, making it rounder than it would otherwise be in a DM-only simulation (Dubinski 1994; Debattista et al. 2008; Abadi et al. 2010; Kazantzidis, Abadi & Navarro 2010; Bryan et al. 2013; Artale et al. 2019; Chua et al. 2019). Another important aspect of the disc–halo relationship, namely the radial evolution of the alignment between

★ E-mail: je.forero@uniandes.edu.co

the stellar disc and the DM halo, has also been explored in some simulations (Bailin et al. 2005; Debattista et al. 2013).

Observational constraints on the DM halo shape have partly been in mutual tension, and have been rapidly evolving during the last decade, hinting that they are affected by substantial systematic uncertainties. One can find studies favouring prolate (Banerjee & Jog 2011; Bowden, Evans & Williams 2016), oblate (Law & Majewski 2010; Deg & Widrow 2013; Vera-Ciro & Helmi 2013) and spherical configurations (Bovy et al. 2016). Constraints from modelling stellar streams discard the prolate configuration (Law & Majewski 2010; Pearson et al. 2015; Bovy et al. 2016) although some other studies still question whether stellar streams can be used to constrain the halo shape once certain assumptions, such as the density profile, are relaxed (Ibata et al. 2013).

In this paper, we analyse the internal DM halo shape in 30 MW-type galaxies from the Auriga project, which are state-of-the-art hydrodynamical simulations of galaxy formation. They have large enough numerical resolution, including an explicit cosmological context, and have appropriate feedback physics to produce realistic MW discs (Grand et al. 2017, 2018a,b). Furthermore, the relatively large number of simulated systems allows us to obtain a handle on the statistical significance of our results.

This paper is structured as follows. In Section 2, we describe the most relevant details of the simulations, and in Section 3, we discuss the method we use to measure the DM halo shape. In Section 4, we present our results focusing on the radial shape trends at $z = 0$, and the alignments with the stellar disc. We place our findings in Section 5 into the context of other numerical work, explore correlations of the shape with baryonic properties in the disc, and finally make a direct comparison against observational constraints for the MW's DM halo shape. We give our conclusions in Section 6.

2 NUMERICAL SIMULATIONS

The Auriga project carries out cosmological zoom-in simulations of MW-sized haloes in a ΛCDM cosmology. The simulations come in two versions: DM only and full baryonic physics included [this entails magnetohydrodynamics (MHD), gas cooling, star formation, black hole growth, and associated feedback processes]. A detailed description of the simulations, the numerical treatment, and the resulting galaxy properties can be found in Grand et al. (2017). Here, we summarize some of the main features.

The simulated objects were chosen as a set of 30 isolated haloes in the DM parent simulation of the Evolution and Assembly of GaLaxies and their Environments (EAGLE) project (Schaye et al. 2015). These haloes were randomly selected from a sample of the most isolated haloes at $z = 0$ whose virial mass M_{200} was between $10^{12}\,\mathrm{M}_\odot$ and $2 \times 10^{12}\,\mathrm{M}_\odot$. The cosmological parameters in the simulations correspond to $\Omega_\mathrm{m} = 0.307$, $\Omega_\mathrm{b} = 0.048$, $\Omega_\Lambda = 0.693$, and a dimensionless Hubble parameter $h = 0.6777$ (Planck Collaboration et al. 2014).

The selected haloes were then re-simulated at much higher resolution by applying a zoom-in technique with variable spatial resolution using the moving-mesh code AREPO (Springel 2010; Pakmor & Springel 2013), and by using a comprehensive model for galaxy formation physics that includes gravity, ideal MHD), a phenomenological description of star formation, chemical enrichment from supernovae and stellar feedback. The simulations also follow the formation and evolution of black holes together with active galactic nuclei (AGNs) feedback.

The 30 zoom-in haloes have a DM particle mass of $\sim 3 \times 10^5\,\mathrm{M}_\odot$, while the baryonic mass resolution is $\sim 5 \times 10^4\,\mathrm{M}_\odot$. The gravitational force softening length for stellar particles and high-resolution DM particles is fixed to be $500\,h^{-1}$ pc in comoving coordinates up to $z = 1$, and 396 pc in physical coordinates afterwards. The gravitational softening length for gas cells changes with the mean cell radius but is limited to be at least the stellar softening length of $500\,h^{-1}$ pc comoving. We refer to this set-up as the 'level-4' resolution, based on the nomenclature of the Auriga project. Six of these haloes were also simulated at a higher 'level-3' resolution, representing an increase by a factor of 8 in mass and a factor of 2 in spatial resolution. We use the higher resolution haloes to define a minimal radius above which our results can be considered converged. From now on we refer to the haloes simulated with baryonic physics as the MHD sample, and to the haloes simulated with DM only as the DMO sample.

3 HALO SHAPE MEASUREMENT

The DM halo shape is usually estimated either based on the isopotential or isodensity surfaces. Observational inferences typically target the isopotential contours that are probed by some dynamical tracers (gas, stars), while simulations more often work with the isodensity contours that can be directly and easily calculated from particle positions. Furthermore, it is well known that the density contours in thin shells are very sensitive to the presence of small satellites (Springel, White & Hernquist 2004). For this reason, we measure the shape by taking volume-enclosed particles, rather than shell-enclosed particles. This method yields results in good agreement to the isodensity contours for radii $\leq$140 kpc as explored by Vera-Ciro et al. (2011).

In particular, we measure the shape using the reduced inertia tensor (Allgood et al. 2006),

$$I_{ij} = \sum_k \frac{x_k^{(i)} x_k^{(j)}}{d_k^2}, \tag{1}$$

where the particle positions are measured with respect to the minimum of the gravitational potential in each halo and are weighted by the inverse of the kth particle distance squared, $d_k^2 = \sum_{i=1}^{3} x_k^{(i)} x_k^{(i)}$, giving each particle the same weight independent of distance.

Diagonalization of this tensor yields the eigenvectors and eigenvalues that approximate the DM halo with an ellipsoidal shape. The axis lengths of this ellipsoid, $a \geq b \geq c$, are the square roots of the eigenvalues, and the directions of the principal axes are the corresponding eigenvectors.

We start the calculations taking into account all particles within a sphere of radius R_initial and then iteratively recompute the triaxial parameters by taking into account those particles within an ellipsoid of semi-axes r, r/q, and r/s, and rescaled distance $d^2 = x^2 + (y/q)^2 + (z/s)^2$, where $q = b/a$ and $s = c/a$ are the previously calculated axes ratios. We repeat this process until the average deviation of the semi-axes is less than 10^{-6}. For the converged shape, we define a single characteristic radius R as the geometrical mean of the axes lengths $R = (abc)^{1/3}$. We use this radial coordinate R to parametrize the spatial changes in halo shape we report in the following sections. This is essentially the same method used to estimate the halo shape in the DM-only Aquarius simulations (Vera-Ciro et al. 2011).

Following the convergence criterion by Vera-Ciro et al. (2011) for DM-only simulations, we restrict the measurement of the ellipsoidal parameters to radii between 1 kpc and R_{200}, where R_{200} corresponds to the viral radius defined as the sphere enclosing 200 times the critical density of the Universe. However, the inner scale is similar to the gravitational smoothing length for stellar particles in our

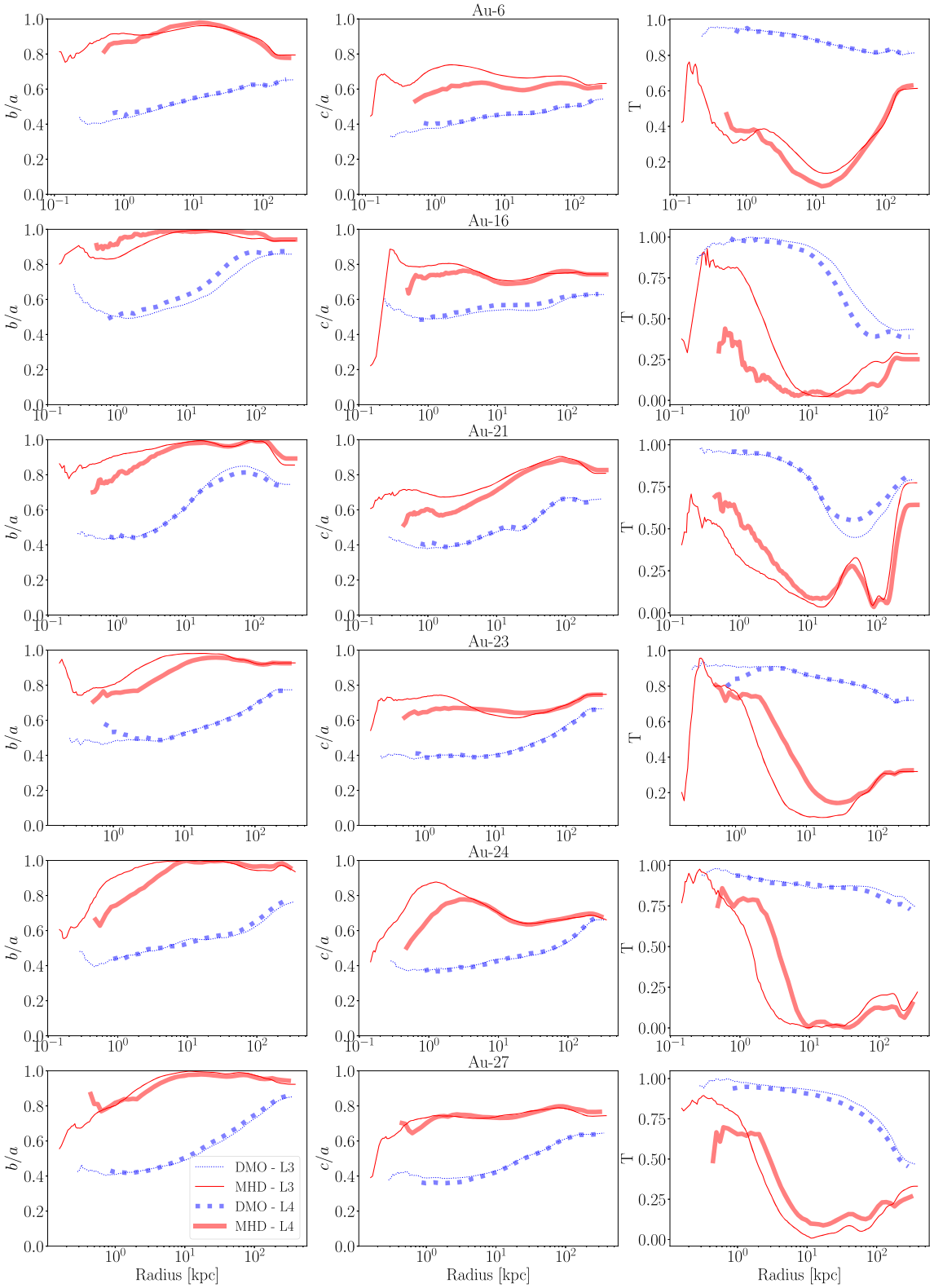

Figure 1. Axes ratios for the six haloes simulated at two different resolutions with two different physical models (DMO and MHD). In DMO simulations there is good agreement between the two resolutions (L3 and L4) at all radii down to scales of ≈1 kpc from the centre. In MHD simulations, there are noticeable differences at scales below ≈10 kpc. In this paper, we only report results at scales larger than ≈16 kpc (R_{200}/16).

Table 1. Axes ratios of Auriga DM haloes at $z = 0$ at different radii in the DMO simulations. The subscripts 16, 8, 4, 2, and 1 indicate that the shape was measured at radii of $R_{200}/16$, $R_{200}/8$, $R_{200}/4$, $R_{200}/2$, and R_{200}, respectively.

Halo	$(b/a)_{16}$	$(c/a)_{16}$	$(b/a)_8$	$(c/a)_8$	$(b/a)_4$	$(c/a)_4$	$(b/a)_2$	$(c/a)_2$	$(b/a)_1$	$(c/a)_1$
Au-1	0.48	0.41	0.52	0.44	0.59	0.48	0.66	0.53	0.72	0.55
Au-2	0.66	0.47	0.72	0.49	0.76	0.51	0.80	0.54	0.79	0.55
Au-3	0.56	0.42	0.61	0.47	0.70	0.55	0.79	0.65	0.85	0.72
Au-4	0.42	0.35	0.47	0.40	0.49	0.43	0.55	0.49	0.59	0.52
Au-5	0.49	0.41	0.53	0.47	0.56	0.51	0.59	0.56	0.66	0.59
Au-6	0.56	0.46	0.58	0.46	0.61	0.49	0.62	0.51	0.65	0.54
Au-7	0.46	0.37	0.45	0.37	0.51	0.40	0.55	0.41	0.62	0.46
Au-8	0.75	0.47	0.84	0.53	0.85	0.58	0.76	0.54	0.82	0.55
Au-9	0.49	0.40	0.52	0.43	0.54	0.45	0.60	0.52	0.65	0.60
Au-10	0.62	0.51	0.61	0.50	0.58	0.49	0.60	0.53	0.65	0.59
Au-11	0.47	0.37	0.36	0.29	0.32	0.28	0.41	0.37	0.47	0.45
Au-12	0.66	0.53	0.76	0.59	0.83	0.66	0.88	0.68	0.94	0.71
Au-13	0.60	0.52	0.61	0.53	0.64	0.54	0.70	0.56	0.73	0.54
Au-14	0.97	0.67	0.95	0.66	0.90	0.64	0.89	0.69	0.87	0.75
Au-15	0.61	0.42	0.65	0.48	0.68	0.52	0.66	0.50	0.70	0.54
Au-16	0.64	0.57	0.73	0.57	0.84	0.58	0.87	0.62	0.88	0.63
Au-17	0.98	0.79	0.98	0.83	0.95	0.84	0.91	0.81	0.93	0.87
Au-18	0.56	0.55	0.57	0.55	0.60	0.57	0.64	0.59	0.62	0.56
Au-19	0.58	0.51	0.59	0.50	0.65	0.54	0.73	0.61	0.80	0.70
Au-20	0.61	0.44	0.68	0.48	0.72	0.51	0.76	0.59	0.81	0.70
Au-21	0.67	0.50	0.75	0.50	0.81	0.61	0.80	0.66	0.74	0.64
Au-22	0.68	0.56	0.71	0.59	0.77	0.63	0.82	0.71	0.83	0.78
Au-23	0.54	0.41	0.58	0.44	0.62	0.49	0.70	0.57	0.77	0.66
Au-24	0.54	0.44	0.57	0.47	0.59	0.49	0.66	0.55	0.75	0.66
Au-25	0.59	0.56	0.66	0.65	0.71	0.66	0.62	0.55	0.69	0.61
Au-26	0.52	0.41	0.58	0.43	0.65	0.43	0.73	0.47	0.75	0.51
Au-27	0.53	0.45	0.61	0.51	0.68	0.56	0.76	0.62	0.84	0.64
Au-28	0.49	0.42	0.49	0.44	0.56	0.48	0.64	0.52	0.74	0.58
Au-29	0.50	0.40	0.56	0.45	0.61	0.48	0.69	0.54	0.72	0.60
Au-30	0.62	0.44	0.77	0.54	0.87	0.58	0.85	0.58	0.75	0.53

default simulations. For this reason, we use the level-3 simulations of Auriga performed at higher resolution to gauge the convergence of the shape measurements in the MHD simulations.

Fig. 1 shows the results for the six haloes available both at level-3 and level-4 resolutions. The dotted lines compare the DMO simulations showing that down to scales of 1 kpc the two resolutions yield very comparable results (Vera-Ciro et al. 2011).

In MHD simulations, the situation is less clean as expected. The shape ratios *b*/*a* and *c*/*a* typically start to differ from each other for different resolutions at radii smaller than 15 kpc, with the exception of Au-27, which shows good agreement of the shape measurements at all radii. For radii larger than 15 kpc, the shape ratios in the two resolutions have a difference of 0.01 on average (0.07 in the worst case), while for the triaxiality the differences are 0.05 on average (0.21 in the worst case). For radii between 1 and 15 kpc the shape ratios differ by 0.03 on average (0.21 in the worst case) and the triaxiality differences are 0.12 on average (0.54 in the worst case). These average differences could be then considered as an uncertainty associated with numerical resolution on the results for each individual halo. In order to have the smallest uncertainty associated with resolution, we concentrate in the following on measurements for radii larger than 15 kpc.

In our results, we express the radius in units of R_{200} in order to have a self-consistent dimensionless radial scale across all haloes. Given the similarity of the virial radii across haloes, each dimensionless radius is closely associated with a physical scale with a certain mean value and small standard deviation. For instance, over the 30 haloes in the sample, a dimensionless radius of unity corresponds to a physical distance of 230 $\pm$ 16 kpc. Finally, we also measure the alignment of the halo shape against the stellar disc angular momentum measured using the 10 per cent oldest stellar particles belonging to the main Subfind structure within the virial radius.

4 RESULTS

Our main measurements for the halo shapes are summarized in Table 1 for the DMO simulations, and in Table 2 for the MHD simulations. These results are computed at five different radii: $R_{200}/16$, $R_{200}/8$, $R_{200}/4$, $R_{200}/2$, and R_{200}. In the following subsections, we discuss the results for the triaxiality, the halo-disc alignment and the correlations with baryonic disc properties in greater detail.

4.1 Triaxiality

In the DMO sample, we find that haloes become rounder with increasing radius. The upper panels of Fig. 2 illustrate this effect. The contours show a projected DM slice while the ellipsoid corresponds to the full 3D shape determination. There we see a highly ellipsoidal halo shape at radii $\approx$3 kpc that becomes less elongated at $\approx$50 kpc.

We summarize this trend in Fig. 3 by plotting the results of all 30 haloes of the DMO sample. The left-hand panel shows every halo in the *c*/*a*–*b*/*a* plane at two different radii, $R_{200}/16$ ($\approx$ 14kpc) and R_{200}. The outer part of the halo is systematically rounder than its

Table 2. Same as Table 1, but for the MHD simulations.

Halo	$(b/a)_{16}$	$(c/a)_{16}$	$(b/a)_8$	$(c/a)_8$	$(b/a)_4$	$(c/a)_4$	$(b/a)_2$	$(c/a)_2$	$(b/a)_1$	$(c/a)_1$
Au-1	0.94	0.65	0.96	0.66	0.96	0.70	0.92	0.68	0.91	0.67
Au-2	0.93	0.61	0.95	0.58	0.96	0.61	0.96	0.65	0.88	0.65
Au-3	0.97	0.66	0.96	0.66	0.94	0.70	0.93	0.76	0.94	0.79
Au-4	0.88	0.77	0.82	0.79	0.80	0.76	0.85	0.79	0.83	0.76
Au-5	0.97	0.79	0.94	0.80	0.92	0.81	0.94	0.82	0.94	0.81
Au-6	0.98	0.60	0.96	0.60	0.92	0.63	0.86	0.63	0.78	0.61
Au-7	0.95	0.66	0.95	0.66	0.97	0.68	0.97	0.69	0.96	0.70
Au-8	0.99	0.59	0.97	0.62	0.92	0.66	0.76	0.57	0.83	0.58
Au-9	0.94	0.75	0.93	0.73	0.92	0.73	0.93	0.79	0.92	0.82
Au-10	0.95	0.85	0.94	0.85	0.93	0.85	0.92	0.82	0.91	0.80
Au-11	0.54	0.49	0.55	0.48	0.61	0.53	0.60	0.53	0.62	0.57
Au-12	0.95	0.77	0.88	0.81	0.90	0.84	0.92	0.81	0.95	0.82
Au-13	0.95	0.88	0.96	0.88	0.98	0.82	0.94	0.76	0.82	0.62
Au-14	0.95	0.75	0.93	0.79	0.91	0.80	0.91	0.79	0.93	0.81
Au-15	0.99	0.67	0.98	0.75	0.94	0.79	0.93	0.81	0.88	0.76
Au-16	0.99	0.69	0.99	0.70	0.99	0.74	0.98	0.76	0.99	0.99
Au-17	0.96	0.79	0.96	0.80	0.97	0.82	0.96	0.83	0.96	0.87
Au-18	0.93	0.76	0.92	0.74	0.86	0.72	0.81	0.71	0.74	0.66
Au-19	0.95	0.67	0.91	0.63	0.89	0.63	0.83	0.64	0.85	0.69
Au-20	0.81	0.58	0.91	0.64	0.95	0.71	0.97	0.78	0.86	0.77
Au-21	0.98	0.74	0.97	0.82	0.97	0.87	0.99	0.88	0.99	0.99
Au-22	0.96	0.84	0.93	0.84	0.93	0.85	0.95	0.87	0.97	0.88
Au-23	0.94	0.65	0.96	0.64	0.94	0.65	0.92	0.69	0.93	0.74
Au-24	0.99	0.67	1.00	0.63	0.99	0.65	0.97	0.68	0.98	0.70
Au-25	0.97	0.71	0.96	0.73	0.86	0.74	0.67	0.64	0.71	0.67
Au-26	0.96	0.76	0.97	0.73	0.97	0.70	0.99	0.68	0.97	0.67
Au-27	0.98	0.73	0.97	0.75	0.97	0.79	0.96	0.79	0.95	0.77
Au-28	0.98	0.82	0.94	0.77	0.88	0.73	0.86	0.74	0.93	0.75
Au-29	0.91	0.81	0.89	0.72	0.87	0.69	0.84	0.68	0.85	0.69
Au-30	0.89	0.73	0.78	0.64	0.69	0.53	0.80	0.58	0.91	0.63

inner region. Nevertheless, the halo shape can still be considered to be prolate at all radii.

A different picture emerges for the MHD sample. There all haloes are rounder than their corresponding DMO version at all radii. The lower panel of Fig. 2 can be directly compared to its MHD counterpart; there we observe how at large radii the hydrodynamic halo becomes oblate and almost spherical. The right-hand panel of Fig. 3 shows the results for the 30 haloes in the MHD sample.

In Fig. 4, we summarize the results at different radii using the cumulative distributions for the triaxiality parameter T, defined as

$$T = \frac{a^2 - b^2}{a^2 - c^2}. \quad (2)$$

The left-hand panel of Fig. 4 shows that in the DMO sample the median triaxiality is larger than two-thirds (a typical value that marks the transition from triaxiality to prolateness) at all radii. Furthermore, this median value increases as we move towards the inner part of the halo. The middle panel of Fig. 4 shows how the trends in the MHD simulations go in the opposite direction with respect to the DMO results. There the median triaxiality is always smaller than one-third (a typical value marking the transition from oblateness to triaxiality) and this median value decreases as we move towards the inner part of the halo.

We now quantify this change in triaxiality at the level of individual haloes. We compute $\Delta T \equiv T_{\rm MHD} - T_{\rm DMO}$ to quantify the change between the triaxiality in the MHD and the DMO simulations. The right-hand panel of Fig. 4 shows the cumulative distribution at the same radii as in the other panels. It is evident that at R_{200} all the haloes have reduced their triaxiality after including baryonic physics. At smaller radii, this general trend continues, although two haloes (Au-11 and Au-17) in our sample increase their triaxiality with baryonic physics. However, this small fraction corresponds to haloes that already were outliers in the DMO sample and had triaxialities around one-third, considerably lower than the mean of the parent sample.

Fig. 5 shows that the principal axis directions also change in the MHD simulations with respect to the DMO counterpart. The major axis are aligned within 30 ± 20 deg on average, while the median and minor axes are aligned within 45 ± 20 and 30 ± 20 deg, respectively. At $z = 0$, the DM halo in the MHD simulations has a weak memory of the directions in the DMO set-up.

4.2 Halo-disc alignments

A common assumption in dynamical models of the MW DM halo is that its minor axis is perfectly aligned with the angular momentum of the stellar disc. Although this is a reasonable assumption due to the stability of the galactic disc in this configuration in simplified models of isolated galaxies, this might not perfectly hold in a full cosmological context. To examine the degree of validity of this assumption, we study in this subsection the alignment between the stellar disc's angular momentum eigenvectors and the DM halo shape.

Fig. 6 shows the results as a function of radius. The most striking feature of this plot is that most of the discs have their angular momentum aligned with the minor axis of the halo, perpendicular

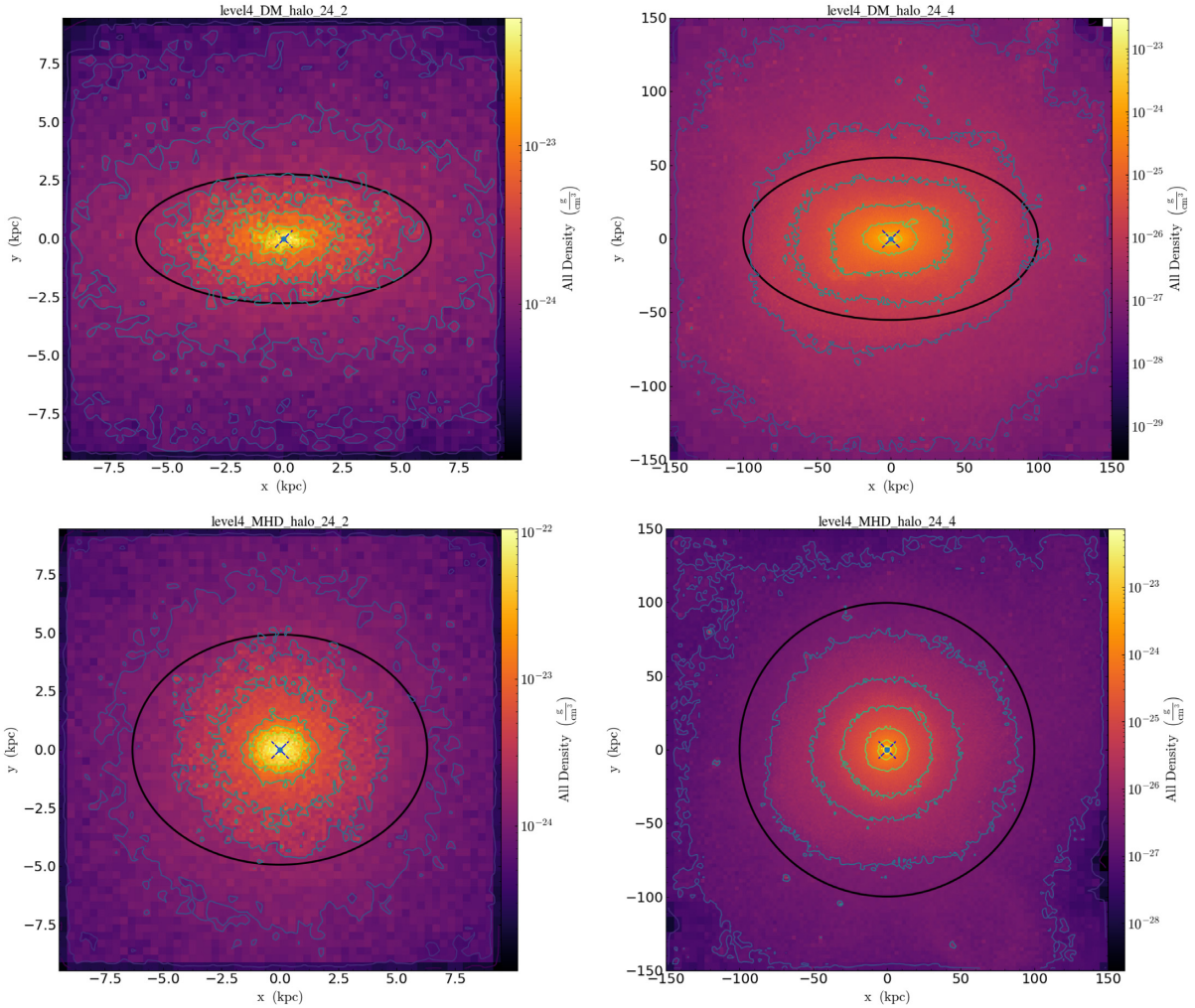

Figure 2. DM density on a logarithmic colour scale within a slice of thickness one tenth of the virial radius. The cut is perpendicular to the short axis of the inertia tensor ellipsoid. The black ellipses show the results of the fitting procedure described in Section 3. Upper/lower panels correspond to DMO/MHD simulations, respectively. Left-hand/right-hand panels show data at small/large radii, respectively. This plot showcases the most noticeable effect in all haloes across the Auriga simulations: haloes become rounder at all radii once baryonic physics is included.

to the intermediate and major axis. The median and the standard deviation of the alignment angles with the major/median/minor axis are 82 ± 14, 82 ± 16, and 19 ± 20 deg, respectively. This confirms statistically the expectation of a galactic disc aligned with the minor axis of its DM halo, although some outliers are present in the sample.

In six haloes, the alignment changes significantly as a function of radius produced by the twisting in the shape ellipsoids. In contrast, the DMO simulations show coherent halo shapes as a function of radius without twisting with the exception of a single halo. Because we are dealing with oblate haloes $b/a \approx 1$, note that the directions corresponding to the medium and major axis could be subject to noise. For this reason, and in order to better quantify the twisting for each halo, we take the standard deviation of the angle with the minor axis, which should be less susceptible to noise. With this measurement, twisting becomes a global property of the halo, as the standard deviation is measured over all the different radii at which we have quantified the alignment.

Fig. 7 shows the correlation between the twisting and the corresponding triaxiality at the four different radii at which the shape directions are measured. The median, mean, and standard deviation of the twisting are 2, 6, and 8 deg, respectively. The correlation between twisting and triaxiality also changes with radius as measured by the Spearman's rank correlation coefficient, a non-parametric way to measure the correlation between two variables; a perfect correlation would be given by a result of $+1$ or -1. The largest correlation is obtained for the halo triaxiality measured at $0.12R_{200}$. The most important consequence of this changing degree of positive correlation is that twisting cannot be explained only by small triaxiality (large asphericity) values and a possibly noisy determination of the shape axis.

4.3 Correlation with baryonic disc properties

The presence of baryons produces rounder DM haloes than found for the corresponding DMO counterpart. To better understand this relationship, we examine the correlation between halo shape and baryonic disc properties. Looking into the measurements already reported by Grand et al. (2017) and Pakmor et al. (2017), we find three baryonic quantities that have the strongest correlation with DM halo triaxiality: the central gas density in a sphere of radius 1 kpc,

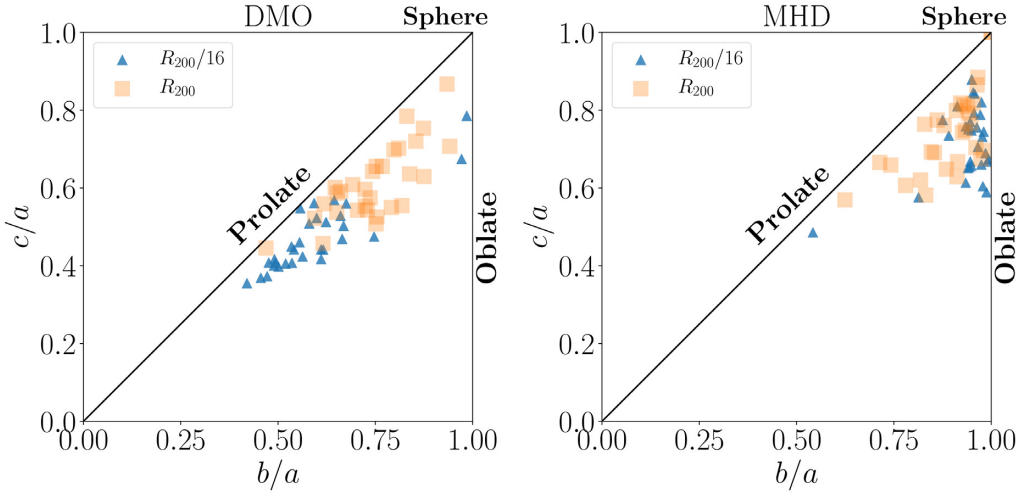

Figure 3. Axes ratios for all simulated haloes. Left-hand/right-hand panel corresponds to DMO/MHD simulations, respectively. Triangles (squares) represent the measurements at $R_{200}/16$ (R_{200}) that correspond to physical distances of ≈14 kpc (≈230 kpc). Here, we visualize three main population trends. First, in DMO simulations haloes are rounder in the outskirts than in the inner part. Secondly, haloes in MHD are rounder in the inner regions than in the outskirts (opposite to the DMO trend). Thirdly, haloes in the MHD simulations are rounder than their DMO counterparts. These three points are further clarified in Fig. 4 through cumulative triaxiality distributions.

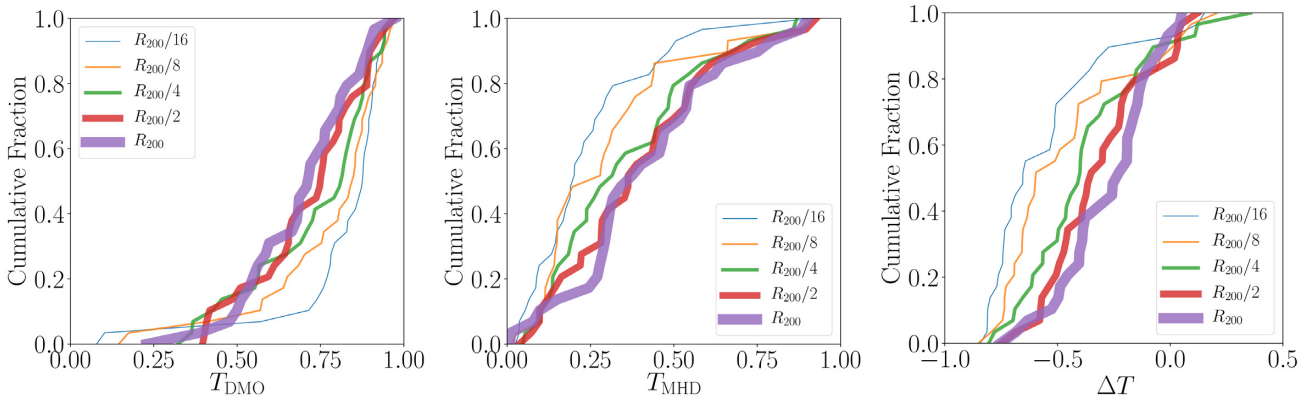

Figure 4. Cumulative distributions of the triaxiality at five different radii. Right/middle panels correspond to the cumulative distribution of triaxiality in the DMO/MHD simulations, respectively. In DMO simulations, the median triaxiality at all radii is larger than two-thirds. Furthermore, the triaxiality increases as one moves towards the inner part of the halo. In MHD simulations, this trend reverses. The median triaxiality at all radii is smaller than one-third, and the halo becomes less triaxial as on moves towards the stellar disc. The right-hand panel shows the cumulative distribution of the changes in triaxiality in simulations with different physics, $\Delta T = T_{\rm MHD} - T_{\rm DMO}$. At the virial radius, all haloes become less triaxial in the MHD simulations, and the change is stronger towards the halo centre. Only two haloes in the sample show the opposite trend of becoming more triaxial (but only at the smallest radii).

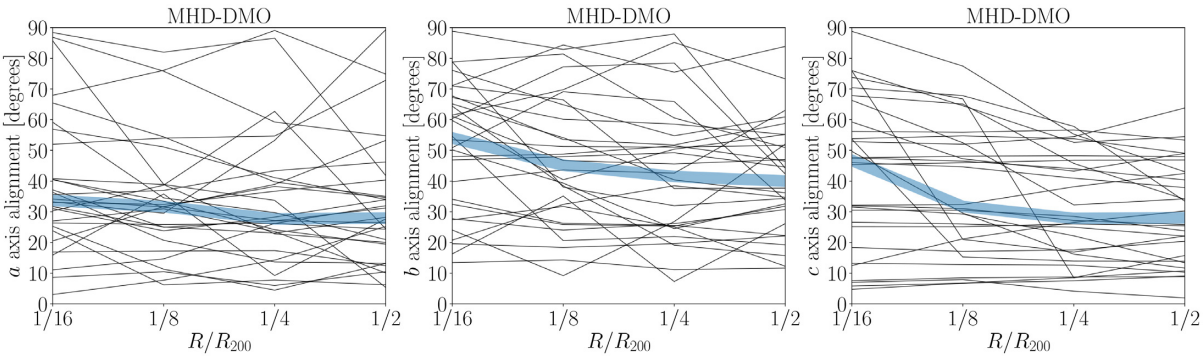

Figure 5. Angles between the principal axis of the DM halo shape in the MHD and DMO simulations as a function of radius. Each panel compares the alignment of the corresponding major, middle, and minor axis in the halo. Thin lines correspond to each one of the 30 haloes in the sample, while the thick line traces the median value as a function of radius. The halo shape in the MHD simulation is weakly correlated to the DMO case.

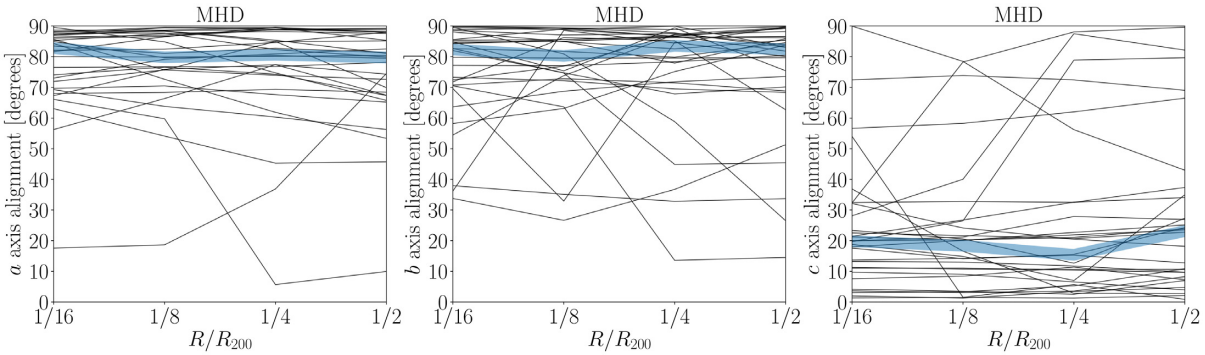

Figure 6. Angles between the principal axis of the DM halo shape and the angular momentum of the stellar disc as a function of the radius at which the halo shape directions are measured. Each panel compares the alignment of the corresponding major, middle, and minor axis in the halo. Thin lines correspond to each one of the 30 haloes in the sample, while the thick line traces the median value as a function of radius. The sample presents a good alignment of the angular momentum with the minor halo axis. This alignment is also constant in radius. However, the DM shells twist significantly in six haloes of our sample making the alignment change.

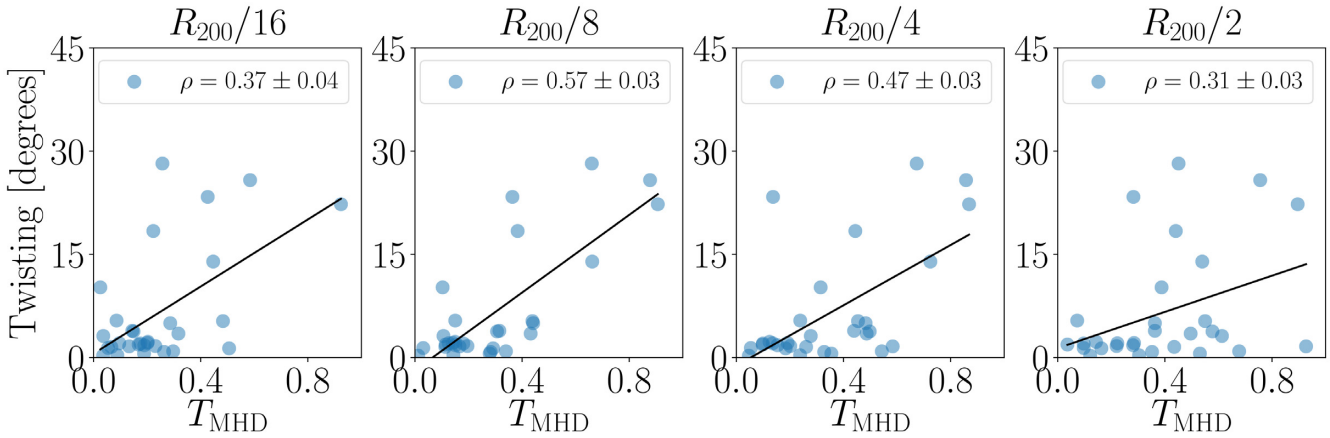

Figure 7. Twisting in the halo-disc alignment (measured as the standard deviation of the alignment angles at four different radii) as a function of the halo triaxiality at the radius indicated in each panel's title. The label with the ρ-value corresponds to the Spearman's rank correlation coefficient (mean value and uncertainty estimated via jackknife resampling), while the line shows the result of a minimum squares fit to the data. Twisting does not correlate with triaxiality in the same way at every radius. The strongest correlation appears around 0.12 R_{200} (28 ± 2 kpc).

the disc to total mass ratio, and the optical radius (the radius at which the *B*-band surface brightness drops below 25 mag arcsec^{-2}).

Fig. 8 shows the correlations of these quantities with the triaxiality at five different radii. We use the Spearmen's rank correlation coefficient to quantify the correlation strength. We find that the strongest correlations are found with the halo shape measured at radii smaller than 0.12 R_{200}. The trend is such that haloes with large triaxiality correlate with high gas density, and stellar discs with low mass and small size. In turn, massive and large stellar discs with low density of gas in their cores correlate with low halo triaxiality.

In Fig. 9, we show the correlation between twisting and the same baryonic properties that showed a high degree of correlation with the triaxiality. In this case, the disc to total ratio does not have a significant degree of correlation. Instead, the disc optical radius and the gas density at the core are the most correlated. The correlation is such that extended stellar discs with a very low gas density at their cores show the most coherent halo shapes.

Recently, Borzyszkowski et al. (2017) used five zoom simulations to report that MW-like DM haloes can be roughly split into two distinct families: stalled and accreting. Stalled haloes assembled early and have remained almost unchanged in the last 7 Gyr, while accreting haloes have been growing constantly. Borzyszkowski et al. (2017) also link the two populations to differences in the DM filaments feeding the haloes. Stalled haloes at $z = 0$ are embedded in a single large thick filament, while accreting haloes are pierced by many thinner filaments. To what extent can the twisting and high triaxiality present in the MHD haloes be linked to this dichotomy?

In Fig. 10, we show the correlation between the twisting and the age of the bulge, the age of the stellar disc, and the DM halo age. We estimate the stellar ages directly as the mean value in the stellar age distribution for each component, while the DM halo age corresponds to the look-back time at which the halo consolidated half of its present mass. In the three cases, we find a correlation between age and twisting that goes in the direction claimed by Borzyszkowski et al. (2017): components with early assembly (i.e. stalled haloes) have a smaller degree of twisting. A detailed study to interpret this with respect to the cosmic web location of the haloes is however beyond the scope of this paper.

5 DISCUSSION

The first prominent effect we found in this paper is that baryons produce significantly rounder DM haloes. This effect has already been widely reported in the literature, and we confirm it here for

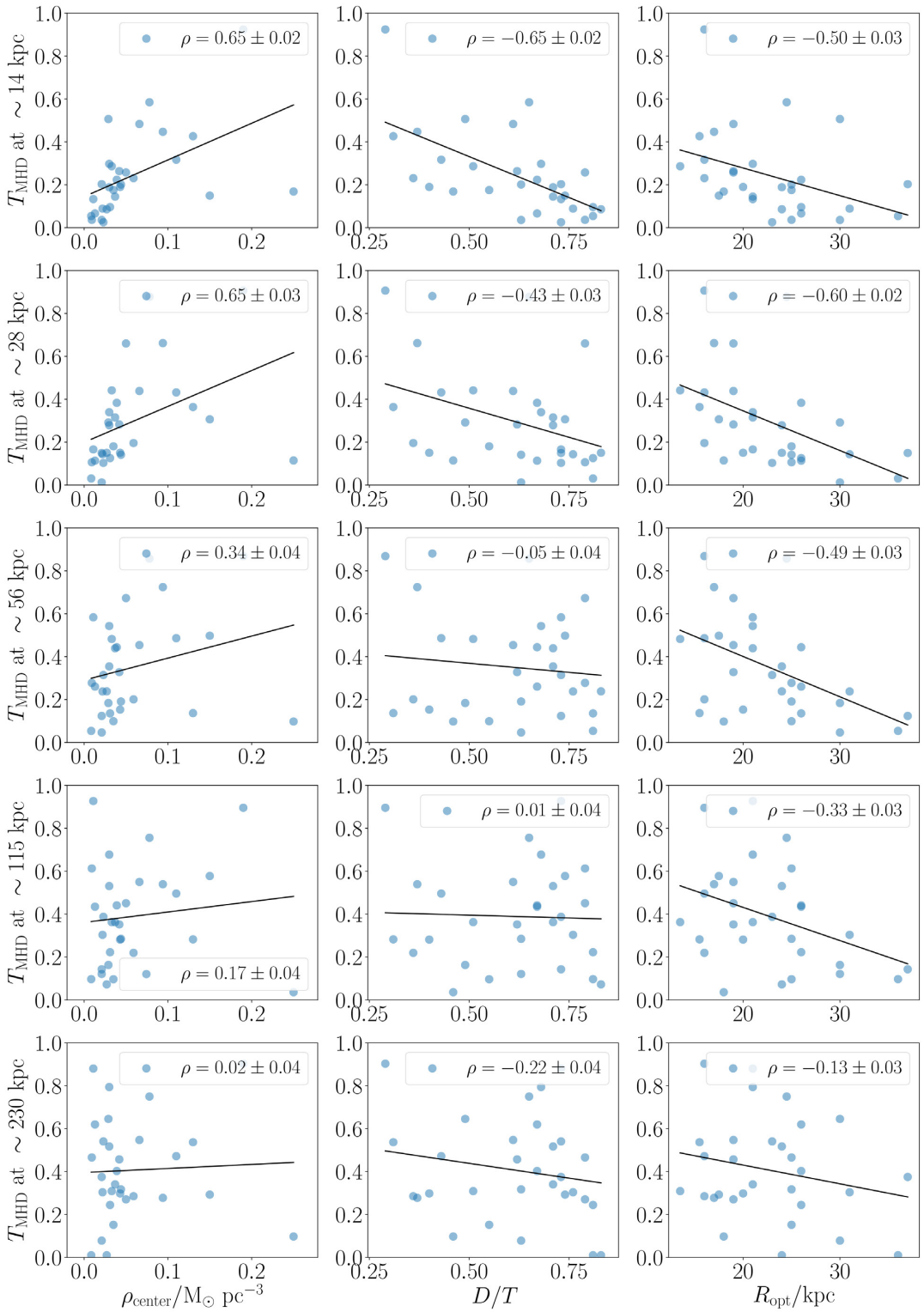

Figure 8. Correlations between the halo triaxiality at different radii and baryonic disc properties. The label with the ρ-value corresponds to the Spearman's rank correlation coefficient (mean value and uncertainty estimated via jackknife resampling). The line is the best minimum squares fit to a line. The x-axis in the first column is the gas density at the centre of the galaxy within a sphere of radius 1 kpc (Pakmor et al. 2017); the second column shows the disc to total mass ratio, and the last column includes the disc optical radius defined to be the radius at which the B-band surface brightness drops below 25 mag arcsec^{-2} (Grand et al. 2017). The largest correlations are found for the two smaller radii (R_{200}/16 and R_{200}/8). Extended and massive stellar discs with a low gas content at their cores are correlated with low DM triaxialities. The correlation decreases as one approaches larger radii.

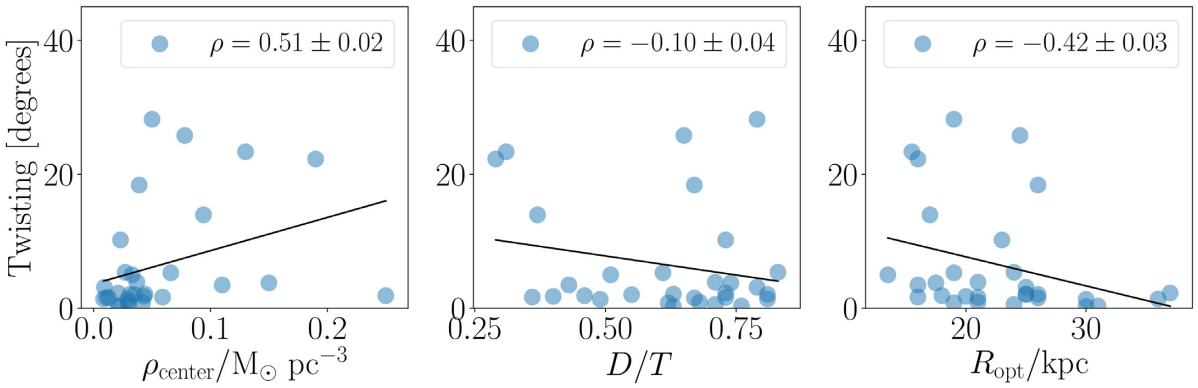

Figure 9. Twisting in the halo-disc alignment as a function of the same baryonic disc properties as in Fig. 8. The label with the ρ-value corresponds to the Spearman's rank correlation coefficient (mean value and uncertainty estimated via jackknife resampling). The line is the best minimum squares fit to a line. In this case, the disc to total mass ratio does not correlate with the alignment twisting. The gas density at the centre and the disc optical radius still show a strong correlation, albeit weaker than the correlation of each with the triaxiality.

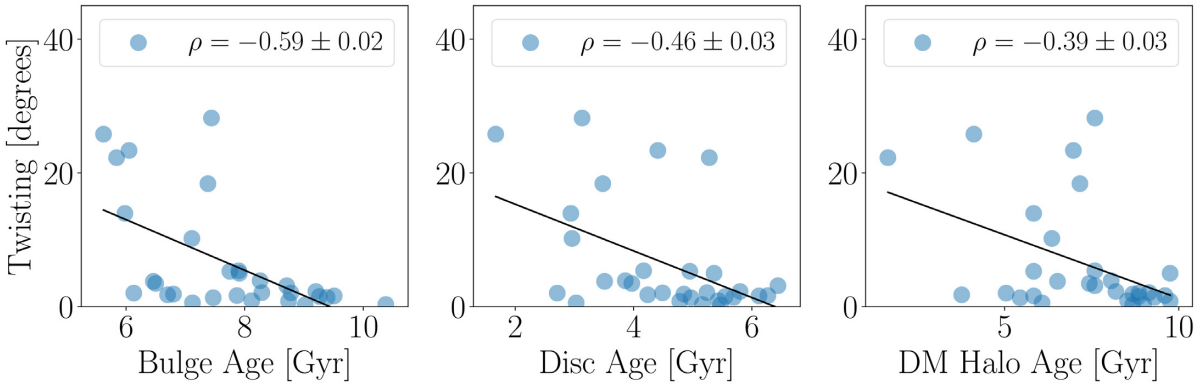

Figure 10. Twisting in the halo-disc alignment as a function of the mean stellar age in the bulge/disc and the look-back formation time of the DM halo (time at which half of its present mass has assembled). The label with the ρ-value corresponds to the Spearman's rank correlation coefficient (mean value and uncertainty estimated via jackknife resampling). The line is the best minimum squares fit to a line.

the Auriga simulations. It has also been found that the strength of the change depends on the numerical resolution, the gas cooling implementation, and the models describing star formation and stellar feedback (Bailin et al. 2005; Debattista et al. 2008; Bryan et al. 2013; Butsky et al. 2016; Artale et al. 2019; Chua et al. 2019). The key concept unifying these results is that the baryon distribution influences and correlates with the DM halo shape. Indeed, as we demonstrated in the previous section on the correlations with disc properties, we find a clear tendency that extended massive stellar discs correlate with spherical DM distributions.

The second part of our findings concerns the disc-halo alignment. The dominant trend is that of a strong alignment between the disc and the DM halo shape at all radii. In six haloes of our sample we find a changing alignment as a function of radius. This implies a twisting in the halo shape as a function of radius. Considering that this effect is virtually absent in our DMO simulations, it is very likely that the detailed radial evolution of the alignments between the disc and the halo depends on the hydrodynamics and feedback implementations.

Twisting has been also reported as an uncommon feature in some simulated systems found in the literature. Jing & Suto (2002) reported it in their DM only simulations as measured through direction changes of large and medium shape axis. They only had three high-resolution MW-like haloes and could not make a statistical statement about the significance of this effect. However, they saw the twisting as an artefact resulting from high values of the *b*/*a* ratios that make the determination of the medium axis noisy, an effect that we have demonstrated can be discarded for our simulations. Bailin et al. (2005) used seven hydrodynamic simulations to study the disc halo alignment as a function of radius. For radii smaller than $0.1R_{200}$, they find a strong global alignment between the halo and the disc. However, in some haloes, at larger radii the angle between the components twists resulting in a weaker correlation between the disc and the halo shape. A more recent study by Velliscig et al. (2015) used the EAGLE simulations to report the median alignment between the stellar and DM components in 1008 galaxies around the MW mass range. Our results agree on the high degree of alignment on average as a function of radius. However, the authors do not mention whether they find any outliers with the kind of twisting we report here.

To finalize, we use the results reported by Law & Majewski (2010) and Bovy et al. (2016) to place our results in an observational context. Law & Majewski (2010) used observations of the Sagittarius tidal stream to constrain the shape of the gravitational potential. They point out that previous studies that assumed an axisymmetric galactic potential were not able to fit all the available dynamic constraints for the Sagittarius stream, motivating their approach of using a rigid triaxial potential with coaxial potential ellipsoids

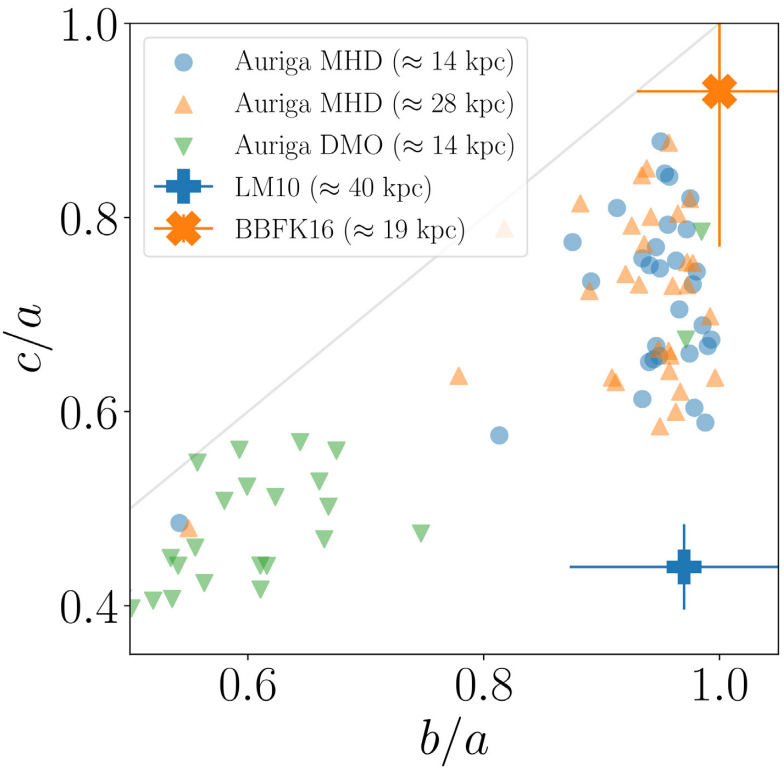

Figure 11. Comparison of our results against observational constraints for the DM halo shape in the MW by Law & Majewski (2010, LM10) and Bovy et al. (2016, BBFK16). We find that one-fifth of the haloes in the MHD sample are consistent with the constraints by Bovy et al. (2016). In contrast, none of the haloes in the MHD and DMO simulations seems to be consistent with the results of Law & Majewski (2010).

for the DM component. Their results constrain the triaxiality of this potential component. They also translate their results into a triaxiality of the density contours (which could be compared against our results) to be $c/a = 0.44$ and $b/a = 0.97$ at a radius of ∼40 kpc. They do not report any uncertainties for these two values. Looking at their plots for the quality of fit criterion as a function of dark halo axial scales (their fig. 5), we choose a conservative 10 per cent relative uncertainty. One surprising element in their results is that the major axis of the halo shape is perpendicular to the stellar disc plane.

The results by Bovy et al. (2016) are based on the same general approach but use instead the GD-1 (Grillmair & Dionatos 2006) and Pal 5 (Odenkirchen et al. 2009) streams to constraint the shape of the DM component of the galactic halo potential. They use general models with many degrees of freedom for the galactic potential in order to measure to what extent these two streams are sensitive to the triaxiality of the DM halo component. The DM component is written directly as a triaxial density profile with coaxial ellipsoids, and the corresponding potential is found by numerical integration. They find that the width of the Pal 5 stream gives $b/a \approx 1$, and therefore fix it to be $b/a = 1$ exactly. Using this value they report their most stringent constraint of $c/a = 0.93 \pm 0.16$ at a radius of ≈19 kpc from the Galactic Centre.

Fig. 11 shows an explicit comparison in the c/a–b/a plane of our findings for hydrodynamic simulations against the results by Law & Majewski (2010) and Bovy et al. (2016). We find six MHD haloes with $b/a < 0.93$ and $c/a > 0.77$ that could be considered consistent with the shape constraints by Bovy et al. (2016), while only one DMO halo outlier is consistent with those constraints. In contrast, none of the simulated haloes (MHD nor DMO) is consistent with the results of Law & Majewski (2010). The change of triaxiality with radius in our simulations cannot account for these two extremely different shape constraints at different radii.

The results by Law & Majewski (2010) would imply that the DM halo of our MW is an extreme outlier in the ΛCDM model. This extreme prolateness also correlates with the extreme triaxiality of the 11 classical satellites of the MW ($c/a \approx 0.2$ and $b/a \approx 0.9$) measured at larger radii, with a spatial distribution also oriented perpendicular to the MW plane, another highly unusual feature in the ΛCDM model (Shao et al. 2016; Forero-Romero & Arias 2018; Shao, Cautun & Frenk 2019). An additional caveat is the presence of the Large Magellanic Cloud that might induce a large enough perturbation (not taken into account in those models) and bias the results (Vera-Ciro & Helmi 2013; Gómez et al. 2015; Peñarrubia et al. 2016).

6 CONCLUSIONS

In this paper, we have measured the shape of 30 isolated MW-sized DM haloes simulated in the Auriga project using the zoom-in technique. The haloes were simulated using two different set-ups: dark matter only (DMO) simulation, and full MHD including star formation and feedback. We applied the shape measurement algorithm by Allgood et al. (2006) to the DM haloes of these simulations to quantify the halo shape as a function of radius, and the degree of alignment between the angular momentum in the stellar disc and the DM halo shape.

We find that MHD haloes are rounder than DMO haloes at all radii. MHD haloes tend towards more oblate shapes, sometimes becoming almost spherical ($T < 1/3$), while DMO haloes are prone to show more prolate shapes ($T > 2/3$). The rounding effect by

baryons is more noticeable as one moves closer to the Galactic Centre, and it strongly correlates with baryonic properties of the disc. More precisely, the triaxiality is smaller for extended and massive stellar discs with low gas densities at their cores.

We also measured the alignment of the halo with the stellar disc's angular momentum at different radii. For the majority of the sample, the angular momentum is strongly aligned with the minor axis of the halo at all measured radii. However, in some haloes the alignment changes noticeably with radius. This alignment evolution implies a radial twisting between the ellipsoids describing the halo shape. We quantify this twist with the standard deviation of the angle between the angular momentum and the halo minor axis at radii below $\leq 0.5\ R_{200}$, and find that younger bulges and higher gas densities correlate with larger twisting values.

We compared our results against two observational constraints for the DM halo shape of the MW. The constraints are at two different radii coming from different observational tracers. We find that 20 per cent of the haloes in the MHD simulations are consistent with the constraints by Bovy et al. (2016) at $\approx$19 kpc, corresponding to an almost spherical halo, while none of the haloes, neither in MHD nor DMO, has overlap with the shape constraints by Law & Majewski (2010) at $\approx$ 40 kpc, which argue for a more oblate shape.

A more complete understanding of the influence of baryons on the different properties we have measured will require at least two more elements. First, a study on how the halo and the disc co-evolved as a function of time. For instance, using DM-only simulations, Vera-Ciro et al. (2011) suggested that the current DM halo shape strongly correlates with the time evolution of the halo as traced by the shape measured at the virial radius. This effect might largely be washed out and no longer hold once baryons are included. The opposite trend of triaxiality in MHD simulation as a function of radius compared to the DMO simulations, together with the twisting effect in some of the haloes, seems to suggest that memory of the historical build-up is at most poorly reflected in the shapes at $z = 0$. The second element to take into account is the effect of the cosmic web (both DM and gaseous) on any evolutionary trend (Forero-Romero, Contreras & Padilla 2014; Borzyszkowski et al. 2017; Ganeshaiah Veena et al. 2019).

We also think that the twisting density shells we find in some of the haloes are a feature that deserves further study, especially in light of attempts to constrain halo shape parameters with tidal stream data. The inclusion of a parametrization describing this degree of twisting might relax the present conflicts between the observational inferences and the numerical results.

ACKNOWLEDGEMENTS

We acknowledge fruitful discussions with Patricia Tissera during the preparation of the manuscript. This project has received funding from the European Union's Horizon 2020 Research and Innovation Programme under the Marie Skłodowska-Curie grant agreement no. 734374.

REFERENCES

Abadi M. G., Navarro J. F., Fardal M., Babul A., Steinmetz M., 2010, MNRAS, 407, 435
Allgood B., Flores R. A., Primack J. R., Kravtsov A. V., Wechsler R. H., Faltenbacher A., Bullock J. S., 2006, MNRAS, 367, 1781
Artale M. C., Pedrosa S. E., Tissera P. B., Cataldi P., Di Cintio A., 2019, A&A, 622, A197
Bailin J. et al., 2005, ApJ, 627, L17
Banerjee A., Jog C. J., 2011, ApJ, 732, L8
Borzyszkowski M., Porciani C., Romano-Díaz E., Garaldi E., 2017, MNRAS, 469, 594
Bovy J., Rix H.-W., 2013, ApJ, 779, 115
Bovy J., Bahmanyar A., Fritz T. K., Kallivayalil N., 2016, ApJ, 833, 31
Bowden A., Evans N. W., Williams A. A., 2016, MNRAS, 460, 329
Bryan S. E., Kay S. T., Duffy A. R., Schaye J., Dalla Vecchia C., Booth C. M., 2013, MNRAS, 429, 3316
Butsky I. et al., 2016, MNRAS, 462, 663
Catena R., Ullio P., 2010, J. Cosmol. Astropart. Phys., 8, 004
Chua K. T. E., Pillepich A., Vogelsberger M., Hernquist L., 2019, MNRAS, 484, 476
Debattista V. P., Moore B., Quinn T., Kazantzidis S., Maas R., Mayer L., Read J., Stadel J., 2008, ApJ, 681, 1076
Debattista V. P., Roškar R., Valluri M., Quinn T., Moore B., Wadsley J., 2013, MNRAS, 434, 2971
Deg N., Widrow L., 2013, MNRAS, 428, 912
Dubinski J., 1994, ApJ, 431, 617
Forero-Romero J. E., Arias V., 2018, MNRAS, 478, 5533
Forero-Romero J. E., Contreras S., Padilla N., 2014, MNRAS, 443, 1090
Gómez F. A., Besla G., Carpintero D. D., Villalobos Á., O'Shea B. W., Bell E. F., 2015, ApJ, 802, 128
Ganeshaiah Veena P., Cautun M., Tempel E., van de Weygaert R., Frenk C. S., 2019, MNRAS, 487, 1607
Grand R. J. J. et al., 2017, MNRAS, 467, 179
Grand R. J. J. et al., 2018a, MNRAS, 474, 3629
Grand R. J. J. et al., 2018b, MNRAS, 481, 1726
Grillmair C. J., Dionatos O., 2006, ApJ, 641, L37
Helmi A., White S. D. M., 1999, MNRAS, 307, 495
Ibata R., Lewis G. F., Martin N. F., Bellazzini M., Correnti M., 2013, ApJ, 765, L15
Iocco F., Pato M., Bertone G., 2015, Nature Phys., 11, 245
Jing Y. P., Suto Y., 2002, ApJ, 574, 538
Johnston K. V., 1998, ApJ, 495, 297
Kazantzidis S., Abadi M. G., Navarro J. F., 2010, ApJ, 720, L62
Law D. R., Majewski S. R., 2010, ApJ, 714, 229
Navarro J. F., Steinmetz M., 1997, ApJ, 478, 13
Odenkirchen M., Grebel E. K., Kayser A., Rix H.-W., Dehnen W., 2009, AJ, 137, 3378
Olling R. P., Merrifield M. R., 2000, MNRAS, 311, 361
Pakmor R., Springel V., 2013, MNRAS, 432, 176
Pakmor R. et al., 2017, MNRAS, 469, 3185
Peñarrubia J., Gómez F. A., Besla G., Erkal D., Ma Y.-Z., 2016, MNRAS, 456, L54
Pearson S., Küpper A. H. W., Johnston K. V., Price-Whelan A. M., 2015, ApJ, 799, 28
Planck Collaboration et al., 2014, A&A, 571, A16
Schaye J. et al., 2015, MNRAS, 446, 521
Shao S., Cautun M., Frenk C. S., Gao L., Crain R. A., Schaller M., Schaye J., Theuns T., 2016, MNRAS, 460, 3772
Shao S., Cautun M., Frenk C. S., 2019, MNRAS, 488, 1166
Sofue Y., Honma M., Omodaka T., 2009, PASJ, 61, 227
Springel V., 2010, MNRAS, 401, 791
Springel V., White S. D. M., Hernquist L., 2004, in Ryder S., Pisano D., Walker M., Freeman K., eds, Proc. IAU Symp. 220, Dark Matter in Galaxies. Astronomical Society of the Pacific, San Francisco. p. 421
Tremaine S., 1999, MNRAS, 307, 877
Velliscig M. et al., 2015, MNRAS, 453, 721
Vera-Ciro C., Helmi A., 2013, ApJ, 773, L4
Vera-Ciro C. A., Sales L. V., Helmi A., Frenk C. S., Navarro J. F., Springel V., Vogelsberger M., White S. D. M., 2011, MNRAS, 416, 1377

This paper has been typeset from a TEX/LATEX file prepared by the author.